Molecular Dynamic and Free Energy Studies of Primary Resistance Mutations in HIV-1 Protease−Ritonavir Complexes

Ornjira Aruksakunwong,[†] Peter Wolschann,[‡] Supot Hannongbua,[†] and Pornthep Sompornpisut*,[†]

Department of Chemistry, Faculty of Science, Chulalongkorn University, Bangkok 10400, Thailand, and Institute for Theoretical Chemistry, University of Vienna, Vienna 1090, Austria

Received March 15, 2006

To understand the basis of drug resistance of the HIV-1 protease, molecular dynamic (MD) and free energy calculations of the wild-type and three primary resistance mutants, V82F, I84V, and V82F/I84V, of HIV-1 protease complexed with ritonavir were carried out. Analysis of the MD trajectories revealed overall structures of the protein and the hydrogen bonding of the catalytic residues to ritonavir were similar in all four complexes. Substantial differences were also found near the catalytic binding domain, of which the double mutant complex has the greatest impact on conformational changes of the protein and the inhibitor. The tip of the HIV-1 protease flap of the double mutant has the greater degree of opening with respect to that of the others. Additionally, the phenyl ring of Phe82 moves away from the binding pocket S1′, and the conformational change of ritonavir subsite P1′ consequently affects the cavity size of the protein and the conformational energy of the inhibitor. Calculations of binding free energy using the solvent continuum model were able to reproduce the same trend of the experimental inhibition constant. The results show that the resistance mutants require hydrophobic residues to maintain the interactions in the binding pocket. Changes of the cavity volume correlate well with free energy penalties due to the mutation and are responsible for the loss of drug susceptibility.

INTRODUCTION

The human immunodeficiency virus type 1 protease (HIV-1 PR) is one of the major targets for the treatment of AIDS. The enzyme is essential for processing the precursor viral polypeptide into a functional protein that is essential for viral assembly and the mature infectious virus.[1−3] HIV-1 PR is a homodimeric protein consisting of two identical polypeptides of 99 amino acids. Many crystal structures of HIV-1 protease complexed with various inhibitors have been solved. The catalytic active site located at the dimer interface (Figure 1) is formed by the catalytic triad residues Asp25-(25′)−Thr26(26′)−Gly27(27′).[4−6] Additionally, the binding site, which is a large hydrophobic cavity, is stabilized by hydrophobic interactions and hydrogen bonding.

The first inhibitors of HIV-1 PR were based on the transition-state structure of the peptidic substrate by replacing the scissile peptide bond with the uncleavable isostere.[7] Recently, there have been nine Food and Drug Administration (FDA)-approved protease inhibitors in clinical uses (indinavir, saquinavir, nelfinavir, ritonavir (RTV), lopinavir, atazanavir, fosamprenavir, amprenavir, and tipranavir). These HIV-1 PR inhibitors bind to the substrate binding site.[8] Ritonavir is a very potent HIV-1 PR inhibitor of wild-type (wt) HIV-1 PR and has high oral bioavailability in humans. It is normally used in combination with other drugs.[5,9]

Unfortunately, the virus evolves under the selective pressure of these inhibitors. They often become clinically resistant, during the first year of monotherapy. On the basis of genotypic and phenotypic resistance testing, more than 87 mutations of HIV-1 PR have been observed in at least 49 positions. Many of them have shown cross-resistance to more than one drug.[8] In particular, the double mutation V82F/I84V has shown high resistance against ritonavir, saquinavir, nelfinavir, indinavir, and amprenavir.[10] The single mutations, V82F and I84V, show major determinants of phenotypic and clinical resistance to ritonavir. These two mutations were classified as primary as they directly confer reduced drug susceptibility. Three-dimensional structures of the V82F/I84V and V82F mutants complexed with symmetric protease inhibitors have been determined by X-ray crystallography.[11] Nevertheless, the crystal structure of the mutant−ritonavir complex is not yet known. Experimental thermodynamic studies of the binding of the drug to the wild-type and to the V82F/I84V HIV-1 protease were investigated by Todd et al.[12] The study indicated that the V82F/I84V mutant shows a decrease of 700-fold of the binding affinity to ritonavir. Additionally, the V82F/I84V mutant reduced dimer stability relative to the autolysis-resistant mutant at pH 7.0. The reduction in drug affinity may be due to the combined effects of mutations on both dimer stability and inhibitor binding.[13] The position of the mutated residues is located at the edges of the active site. It makes direct contact with the inhibitors, particularly, the subsites P1 and P1′. Substitution between hydrophobic residues with different bulkinesses of the side chain may distort the wild-type geometry without changing its polarity or chemical composition. Therefore, the mutations represent an excellent candidate for a study of the structure in the binding sites and their changes leading to drug resistance. A structural study of the protein will provide a

* Corresponding author tel.: 662-2187603; fax: 662-2187603; e-mail: pornthep.s@chula.ac.th.
[†] Chulalongkorn University.
[‡] University of Vienna.

10.1021/ci060090c CCC: $33.50
Published on Web 08/24/2006

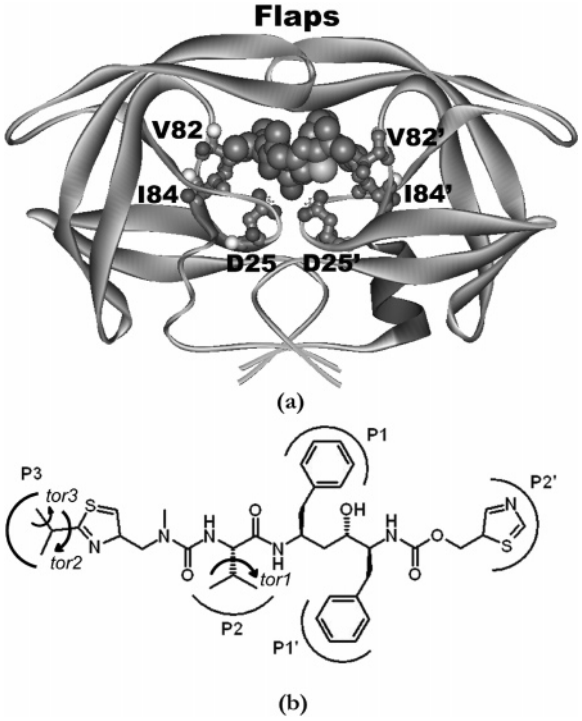

Figure 1. Schematic representation of wild-type HIV-1 protease complex (a) and ritonavir (b). In a, the catalytic residues Asp25/Asp25′ and the mutated residues V82/V82′ and I84/I84′ are shown by the ball-and-stick model, and ritonavir is shown by the space-filled model. The inhibitor side chains denoted by P1, P2, P3, P1′, and P2′ correspond respectively to the substrate binding pockets denoted by S1, S2, S3, S1′, and S2′.

basis for understanding molecular mechanisms of HIV drug resistance, which will be useful for designing anti-HIV inhibitors to combat AIDS.

In this study, we investigated structural and dynamics properties of the primary HIV-1 resistance against ritonavir using molecular dynamic (MD) simulations. The simulations were carried out for the wild-type, V82F, I84V, and V82F/I84V HIV-1 protease complexed with ritonavir in an explicit aqueous solution. The MD approach has provided insightful information on the enzyme−substrate interactions and binding conformations. In addition, the free energy of binding was performed using the molecular mechanics Poisson−Boltzmann surface area (MM/PBSA) approach. The MM/PBSA method offers an efficient computation in calculating the binding free energy of biomolecular systems. It has been extensively used to explore many receptor−drug complexes.

METHODS

Starting Structure. The structures of the HIV-1 protease−RTV complex include the wt, two single mutants (V82F and I84V), and a double mutant (V82F/I84V). The 1.8 Å resolution crystallographic structure of the wt HIV-1 PR−RTV complex (PDB entry 1HXW) was used as the initial structure.[5] All missing atoms and hydrogens of the enzyme were added using the LEaP module in the AMBER 7 package.[14] Because the X-ray structure of the mutants is unknown, the comparative models of V82F, I84V, and V82F/I84V were therefore constructed using the wt model as the template. According to the pK_a calculation, the ionization states of all ionizable residues computed by the University of Houston Brownian Dynamics program[15] were assigned to their common charge, that is, Glu^{-1}, Asp^{-1}, Lys^{-1}, and Arg^{+1}, except for the catalytic Asp25.[16,17] The single protonation at the Asp25 residue has experimentally and theoretically been observed for a number of the HIV-1 protease−inhibitor complexes, particularly, the inhibitor containing the hydroxyl−ethylene isostere.[18,19] In this study, one of the two aspartyl residues Asp25/25′ of the enzyme was assigned as a neutral state. Thus, the four simulated systems were in the monoprotonation state.

The force-field parameters for RTV, which are not available in the AMBER package, were obtained as follows. Hydrogen atoms were added to the X-ray structure (1HXW) containing the RTV atomic coordinates. Then, partial geometric optimization of the hydrogen was performed at the Hartree−Fock level with the 6-31G** basis function using the Gaussian 98 program.[20] Subsequently, electrostatic potentials were generated on the optimized structure. Atomic charges of the inhibitor were calculated by the RESP fitting method.[21] Partial atomic charges and force-field parameters for the inhibitor were generated by the Antechamber suite.[22]

Each complex was immersed in a 10 Å radius of the TIP3P water model.[23] The crystallographic water molecules were kept in the system. Counterions were added to neutralize the system using the LEaP module. In all systems, the total number of water molecules in the $83 \times 72 \times 64$ Å^3 periodic box was 9027 molecules.

Molecular Dynamics Simulations. Energy-minimization and MD simulations were performed using the SANDER module of AMBER 7.0[14] with the Cornell force field.[24] First, energy minimization was applied for water molecules using 500 steps of the steepest descents and then 500 steps of the conjugate gradients. Subsequently, the whole systems were subjected to energy minimization with 1000 steps of the steepest descents and 1500 steps of the conjugate gradients.

The MD simulation was performed employing the periodic boundary condition with the NPT ensemble. A Berendsen coupling time of 0.2 ps was used to maintain the temperature and pressure of the systems.[25] The SHAKE algorithm[26] was employed to constrain all bonds involving hydrogens. A simulation time step of 2 fs was used. All MD simulations were run with a 12 Å residue-based cutoff for nonbonded interactions, and the particle-mesh Ewald method was used for an adequate treatment of long-range electrostatic interactions.[27]

The MD simulation consists of thermalization and equilibration. During the 0−60 ps timeframe, the temperature of the system increased from 0 to 298 K using constant number of particles, volume, and temperature (NVT) conditions. Then, the temperature was maintained at 298 K during equilibration employing constant number of particles, pressure, and temperature (NPT) conditions. The reference pressure and temperature were set to 1 atm and 298 K, respectively. The MD trajectories were collected every 0.1 ps. The convergence of energies, temperatures, and pressures of the systems, and the atomic root-mean-square deviation of the enzyme and the inhibitor (RMSD), were used to verify the stability of the systems. The series of snapshots between 1.5 and 3 ns of the equilibrium phase was used for free energy calculations and structure evaluation.

Calculation of the Binding Free Energy (ΔG_{bind}). In general, the binding free energy of a protein−ligand complex (ΔG_{bind}) is defined as

$$\Delta G_{\text{bind}} = G_{\text{complex}} - (G_{\text{receptor}} + G_{\text{ligand}}) \quad (1)$$

where G_{complex}, G_{receptor}, and G_{ligand} are the free energies of the complex, the protein, and the ligand, respectively.

For each system, the free energy can be estimated in terms of the molecular mechanic potential energy (E^{MM}), the solvation free energy (G_{solv}), and the entropic contribution (TS) as follows:

$$G_{\text{bind}} = E^{\text{MM}} - \text{TS} + G_{\text{solv}} \quad (2)$$

$$E^{\text{MM}} = E_{\text{internal}} + E_{\text{elec}} + E_{\text{vdW}} \quad (3)$$

$$G_{\text{solv}} = G_{\text{elec,solv}} + G_{\text{nonpolar,solv}} \quad (4)$$

where E_{internal} includes the bond, angle, and torsional angle energies; E_{elec} and E_{vdW} are intermolecular electrostatic and vdW energies, respectively. Therefore, E^{MM} is associated with the enthalpic changes in the gas phase upon binding. G_{solv} is composed of electrostatic $G_{\text{elec,solv}}$ and nonpolar $G_{\text{nonpolar,solv}}$ contributions to solvation. The former can be obtained by solving the Poisson−Boltzmann equation,[28] while the latter is approximated on the basis of the solvent-accessible surface area using the hard-sphere atomic model.[29]

The calculation of ΔG_{bind} values of HIV-1 protease−ritonavir complexes was carried out using the MM/PBSA module in AMBER 7. E^{MM} was computed with no cutoff. The electrostatic solvation energy was computed using the Poisson−Boltzmann solver implemented in the Delphi 4 program.[30] The grid spacing was set to $^1/_3$ Å. The Debye−Huckel potentials were employed. The dielectric constants of protein and water were set to 4.0 and 80.0, respectively. The atomic charges of the protein were taken from the Cornell force field.[24] The nonpolar solvation contribution is estimated as

$$G^{S}_{\text{nonpolar,solv}} = \gamma A + b \quad (5)$$

where A is the solvent-accessible surface area and the solvation parameters, γ and b, are 0.00542 kcal/mol Å^2 and 0.92 kcal/mol, respectively. The probe radius of the solvent was set to 1.4 Å. The atomic radii of the solute were taken from the PARSE parameter set.[29]

Considering the entropic effects, structural reorganization and solvent entropy are important contributions in enzyme−ligand bindings. However, a number of studies published by Kollman and Kuhn and Warshel's group showed that this effect is minor for some protein complex systems.[31,32] In the case of HIV-1 protease, a thermodynamic study of four FDA-approved drugs, including indinavir, nelfinavir, saquinavir, and ritonavir, showed that the experimental $T\Delta S$ values of V82F/I84V are ~0.7 kcal/mol less favorable than that of the wild type.[12] On the basis of the information, the entropy difference between the wild type and the three mutants complexed with the same inhibitor should be very small. Normal-mode analysis (NMA) is useful to estimate entropic changes of the solute molecule, but the calculation is considered problematic and time-consuming. In addition, this approach does not take the solvent entropy into consideration. For the above reasons, NMA would not greatly improve the correlation between the experimental K_i and the binding free energy. Thus, the calculation of the solute $T\Delta S$ term has been omitted in the study.

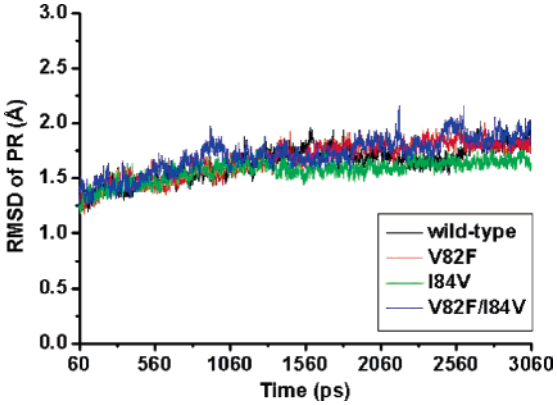

Figure 2. Plot of RMSDs versus the time for the wild-type, V82F, I84V, and V82F/I84V complexes. The obtained RMSD was computed using the structure at $t = 0$ as a reference.

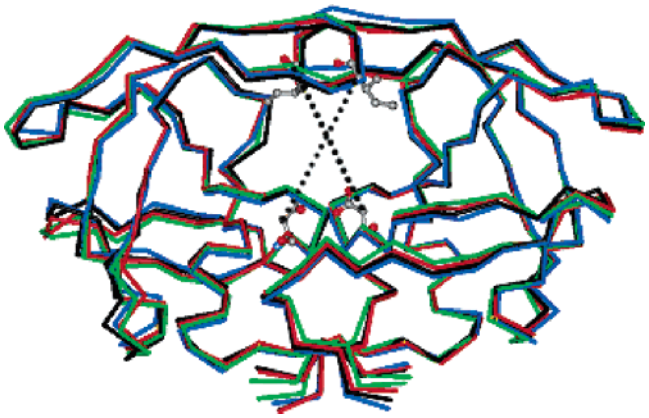

Figure 3. Cα trace of the wild type (black) and V82F (red), I84V (green), and V82F/I84V (blue) mutants. Asp25, Asp25′, Ile50, and Ile50′ are displayed in the ball-and-stick. Dashed lines demonstrate the measured distances of Cα−Ile50/Cβ−Asp25 and of Cα−Ile50′/Cβ−Asp25′. A small panel shows the average RMSD per residue of the mutant structures compared to the wt structure.

RESULTS AND DISCUSSION

The 3 ns MD trajectories of four systems consisting of the wild-type, V82F, I84V, and V82F/I84V HIV-1 PR complexed with ritonavir were generated. The atomic RMSD of the protein structure is shown in Figure 2. The small RMSD fluctuation and the convergence of energies, temperatures, and pressures of the systems during a course of the simulations indicated well-behaved systems.

Structural Features of the HIV-1 Protease. Structures of the wt and all three mutants taken from a snapshot of the MD trajectories are almost identical (Figure 3). From a RMSD comparison, the global tertiary structures of all four systems are similar to each other. The structure of the catalytic triad residues of all three mutants is essentially identical to that of the wt with RMSD < 0.5 Å (data not shown). However, a large RMSD difference can be seen on the HIV flaps of chain B (49′−54′) in the V82F/I84V mutant.

The degree of the flap change is simply demonstrated by a measure of the inter-residue distances of Cα−Ile50/Cβ−Asp25 (chain A) and of Cα−Ile50′/Cβ−Asp25′ (chain B). The distance separation was calculated by taking structures from the MD trajectory and then statistically analyzed as a

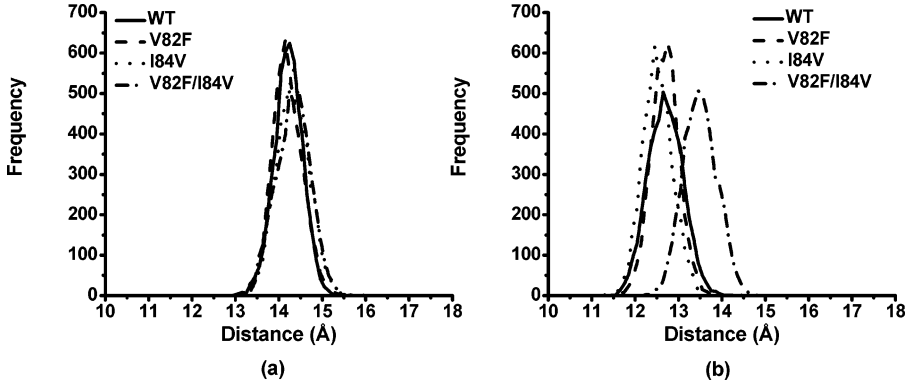

Figure 4. Distributions of the Cα−Ile50/Cβ−Asp25 (a) and the Cα-Ile50′/Cβ-Asp25′ (b) distances (for details, see text and labels in Figure 3) sampled during the 1.5−3 ns timeframe.

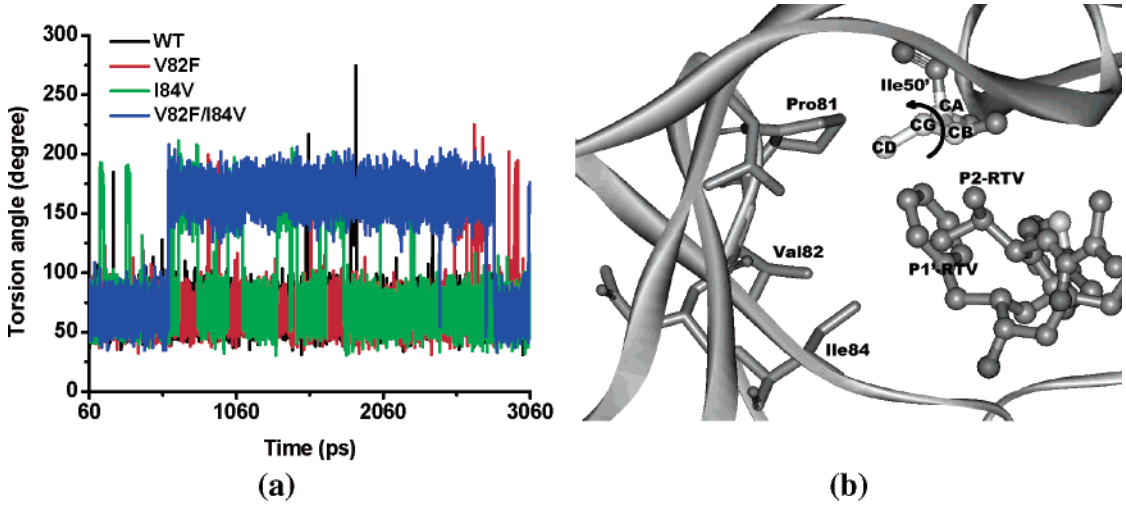

Figure 5. (a) Trajectory of Ile50′ torsion defined by the Cα−Cβ bond (arrow in b). (b) Ile50′, ritonavir, and residues 81−84 of the wild-type HIV-1 PR.

population frequency. From Figure 4, distance distribution peaks of the wt and the mutants are mostly overlying for chain A, while those for chain B are not (Figure 4). A slight shift of the inter-residue distance of chain B was observed for the single mutants, but a greater change was found for the double mutant within a range of 1.0−1.5 Å. This suggests the flap structure may have changed because of the mutation. The most shifted distance was found for the double mutant, and the change of the flap structure of chain A is not equal to that of chain B. It has been known that the inhibitor is not symmetric. It is likely that the flap tip of the double mutant has a greater degree of opening than that of the others. This may relate to a loss of interactions of the drug in the binding pocket of HIV-1 V82F/I84V protease as compared with that of the wt and the V82F and I84V mutants.

A number of MD studies published previously have reported large conformational changes of the flap.[33] The MD simulations of the apo wild type and the apo V82F/I84V mutant of HIV-1 protease observed more frequent and more rapid curling of the flap tip in the mutant than in the wild type. Moreover, the mutant's flap also opened farther than the wild type's, implying more flexibility of the mutant. The flexibility of the flap is highly dependent on the availability and type of ligands.

It appears that the Ile50′ side chain of chain B is in close contact with P1′ and P2 subsites of RTV and residues 81−84 of chain A (Figure 5b). One should note that the interactions in this binding pocket are formed by the hydrophobic packing of side chains. Thus, the shape and size of the substituted nonpolar side chains of V82F and I84V are responsible for the binding of the drug. Detailed attention was focused on residues 50′, 82, and 84 as well as on the inhibitor subsites. The trajectories of the side chain torsions χ_1(Ile50′) and χ_1(Phe82) defined by the Cα−Cβ bond are shown in Figure 5. For Ile50′, the majority of the χ_1 torsion is in a range of 50−90° for the wt and V82F proteases. This suggested no substantial change of Ile50′ side chain. On the other hand, the χ_1(Ile50′) in the I84V and V82F/I84V mutants produces two distinct values with a difference of ∼120°, implying two preferable conformations of Ile50′. The two phenyl rings of Phe82 and Phe82′ in the V82F/I84V mutant have similar χ_1 torsions, while they are significantly different for the V82F mutant. This discrepant side chain orientation of Phe82 implies different interactions between the V82F and the V82F/I84V mutants and the inhibitor.

Conformational Flexibility of Ritonavir. From the simulations, a fluctuation of the RTV structure compared to the X-ray structure exhibits RMSDs of 1.25 ± 0.24, 1.43 ± 0.21, 1.28 ± 0.18, and 1.78 ± 0.13 Å for the wt, V82F, I84V, and V82F/I84V, respectively. The RMSD fluctuation of RTV subsites P1, P2, P3, P1′, and P2′ is shown in Figure 6.

The RMSD plots show that the phenyl ring of P1 (green) and P1′ (blue) and the thiazol ring of P2′ (sky-blue) do not

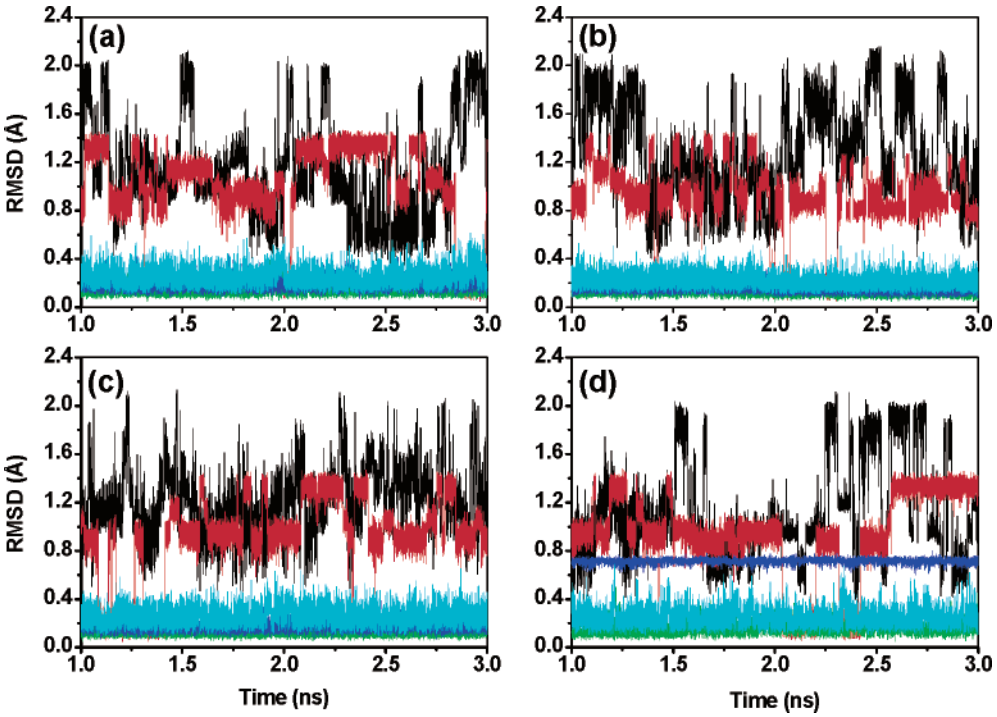

Figure 6. RMSDs of each ritonavir subsite with respect to the starting structure versus the simulation time for the wild type (a) and V82F (b), I84V (c), and V82F/I84V (d) mutants. P3, P2, P1, P1′, and P2′ subsites are given in black, red, green, blue, and sky-blue lines, respectively.

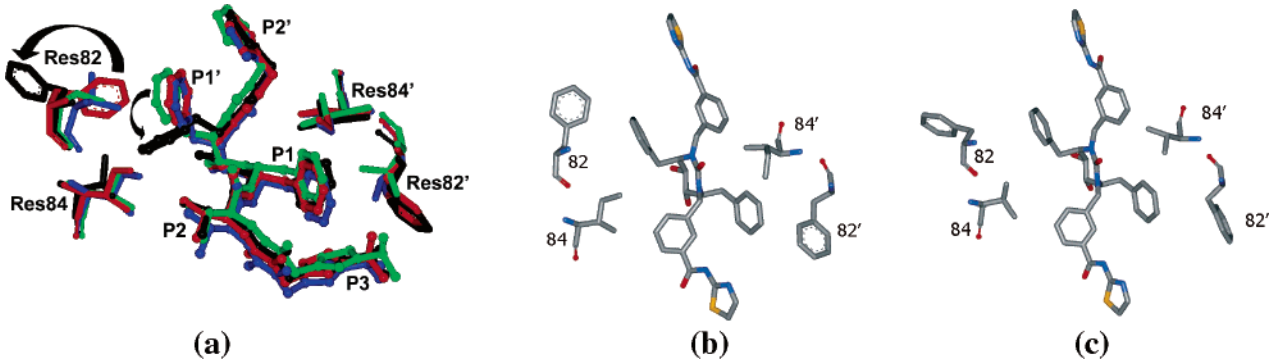

Figure 7. Structure comparison of residues 82 and 84 and ritronavir in HIV-1 protease: (a) the MD structures of the wild type (blue), V82F (red), I84V (green), and V82F/I84V (black); (b and c) the X-ray structures of the V82F (1BV7) and the V82F/I84V mutants (1BWA), respectively. Arrows show different orientations of the phenyl ring of the P1′ and of Phe82 between the single and double mutants.

change their conformation significantly during the simulations, except for the P1′ of the V82F/I84V system. This indicated that the inhibitor side chains of the bound RTV in the binding pocket of the enzyme are considerably rigid. Meanwhile, P3 (black) and P2 (red) side chains show a larger degree of atomic displacements. These are due to the rotation of the two methyl groups of the isopropyl chain. Thus, the flexibility of these subsites is relatively higher upon binding. It appears that the most significant difference between the wt and the mutants was found at the P1′ subsite of RTV. The RMSD change in the double mutant is higher than that in the wt and the two single mutants. This indicates that there is a greater degree of conformational change of the P1′ phenyl ring taking place on the V82F/I84V complex only.

Conformational changes of the P1′ phenyl ring in the double mutant are illustrated in Figure 7a. The P1′ rings in the wt and in the two single mutants remain largely similar to each other, while that in the double mutant is oriented differently. Additionally, the ring orientation of Phe82 of V82F is apparently different from that of the V82F/I84V mutant. Nevertheless, an arrangement of Phe82 side chain was found to be similar to the crystal structures of the single and double mutations of HIV-1 protease (Figure 7b,c).

It should be noted that the ring rearrangement of the P1′ subsite in the V82F/I84V complex has consequently affected the binding pocket S1′ of the protein and the conformational energy of the inhibitor. In the V82F/I84V complex, the side-chain rearrangements of Phe82 coupled with the smaller side chain of Val84 create a larger gap of the S1′ pocket (Figure 7). The volumes of the binding cavity calculated using the CAST program[34] are shown in Table 1. The order of the cavity volumes for all four complexes is V82F/I84V > I84V > wild type > V82F. Apparently, the mutation in V82F/I84V has the largest impact on the volume change in the binding cavity of the protein. This may decrease direct contact between RTV and the residues in the binding pocket S1′. On the contrary, the inhibitor-binding site of the single V82F mutant becomes more restricted as the size of the cavity shrinks because of the bulkiness of the group. This

Table 1. Calculated Volume in the Binding Cavity of the Protease Complexes

complexes	cavity[a] (Å^3) volume (Å3)	ΔV^b (Å^3)
wild type	1257 ± 80	
V82F	1241 ± 84	−16
I84V	1317 ± 59	60
V82F/I84V	1472 ± 55	215

[a] Because the cavity volume was obtained from the MD trajectory, the average value and standard deviation are reported. [b] Change of the cavity volumes (V) calculated from V(wild type) − V(mutant).

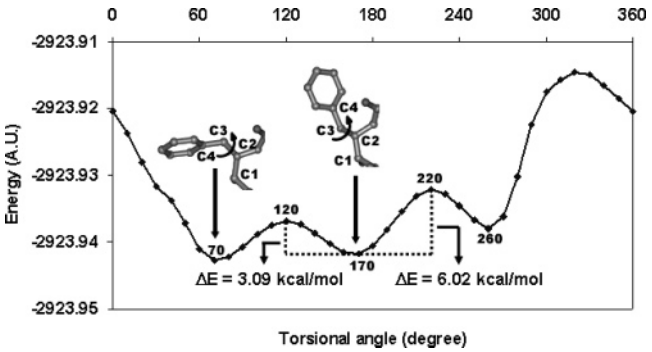

Figure 8. HF/6-31G potential energy versus RTV conformations defined by the C2−C3 torsion of the P1′ side chain.

possibly causes the P1′ ring to remain unchanged in the V82F complex.

A question may arise whether residue 82′ in another subunit of the double mutant and the P1 ring of the inhibitor undergo similar conformational changes. The fact is that RTV is an asymmetric inhibitor; thus, the distinct binding mode in the second monomer is not uncommon. From the simulations, the substituted residues of the protein and the P1′ change of the inhibitor did not significantly alter the conformation of Phe82′ and the P1 ring. In conclusion, the conformation perturbation of residue 82 took place only on one subunit of the HIV-1 protease.

The conformational energy of RTV was investigated by calculating the intramolecular potential energy with various conformations of the P1′ subsite. We began with a starting structure of RTV taken from the MD snapshot, and then, the C1−C2−C3−C4 torsion defined for the conformation of the P1′ phenyl ring (Figure 8) was subjected to change from 0 to 360°. The single-point energy calculations to the whole RTV structure were performed on each generated conformation at the HF/6-31G level. A plot of the calculated potential energy versus RTV conformations at the scanned torsional angles (Figure 8) indicates three minimum potential energies with torsions of 70, 170, and 260°. The results are in good agreement with the P1′ torsions determined from the MD simulations (Figure 7). The lowest total energy corresponds to the RTV conformer in the V82F/I84V complex, while the minimum at 170° is close to the conformer found in the wt and the two single mutants. It should be noted that in the simulations the starting RTV conformer for all systems was ∼170° corresponding to the second energy minimum. The rearrangement of the P1′ ring in the double mutant can overcome the energy barrier of ∼3 kcal/mol to reach an energetically more favorable state; although, the lowest energy of the conformation is about 0.5 kcal/mol lower than the second minimum. This conformation change might relax the strain around the P1′ subsite due to the steric conflict of the V82F/I84V mutant.

Ritonavir−HIV-1 Protease Binding Energy. Table 2 shows the estimated binding free energy (ΔG_{bind}) averaged over the trajectory for each complex. Our calculations show a good correlation with experimental results. A net loss of ΔG_{bind} in the mutant complexes with respect to the wt corresponds to a decrease in the inhibition potency. The

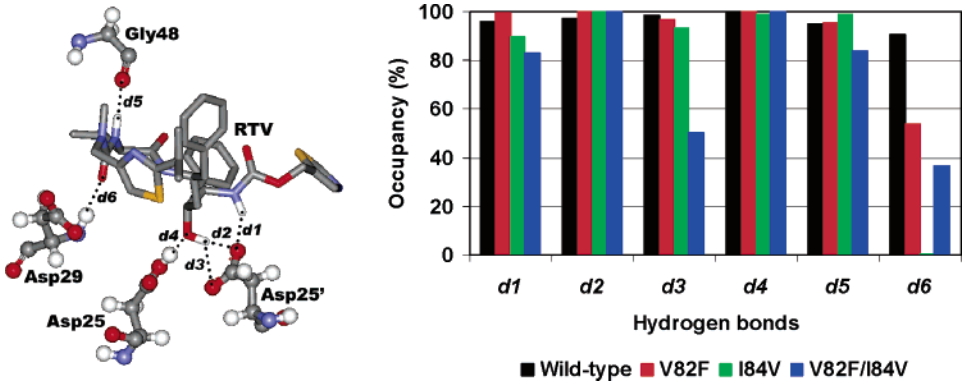

Figure 9. Hydrogen bonding (d1−d6) between HIV-1 PR and ritonavir and the percent occurrence of the corresponding hydrogen bonds calculated from the MD trajectories.

Table 2. Averaged Energy Contributions (kcal/mol) to the Binding Free Energy for Wild-Type and Mutant HIV-1 Protease−Ritonavir Complexes

energy	wild-type	V82F	I84V	V82F/I84V
ΔE_{vdW}[a]	−75.83 ± 3.81[b]	−76.28 ± 4.91	−69.81 ± 4.44	−68.89 ± 4.00
ΔE_{elec}[c]	−52.59 ± 4.76	−49.35 ± 5.09	−47.93 ± 4.67	−44.07 ± 5.26
$\Delta G_{elec,solv}$[d]	23.63 ± 1.67	24.52 ± 1.96	23.40 ± 1.63	20.89 ± 1.05
$\Delta G_{nonpolar,solv}$[e]	−6.29 ± 0.18	−6.31 ± 0.28	−5.93 ± 0.36	−5.82 ± 0.41
ΔG_{bind}[f]	−111.08 ± 4.89	−107.43 ± 6.11	−100.27 ± 4.21	−97.90 ± 2.40
$K_i^{experiment}$(nM)[g]	0.17	0.14	1.90	119

[a] Van der Waals energy. [b] Standard error of the mean. [c] Electrostatic energy. [d] Electrostatic contribution to solvation. [e] Nonpolar contribution to solvation. [f] Binding free energy in the absence of entropic contribution. [g] The experimental inhibition constant.

calculated difference in free energy of binding between the wt and each mutant is −3.65 kcal/mol for V82F, −10.81 kcal/mol for I84V, and −13.18 kcal/mol for V82F/I84V. This suggested that the binding affinity of RTV is strongest for the native protein and becomes less favorable in the mutants. Particularly, biochemical data indicated that RTV has about 700 times lower of an inhibition constant (K_i) value with the double mutant. All complexes are correctly rank-ordered, although the magnitudes of ΔG_{bind} are overestimated.

A detailed analysis suggested that there is a decrease in both van der Waals and electrostatic contributions in the mutants upon binding. It appears that for all complexes van der Waals interactions are the largest contribution to the binding free energy (∼70%). This explains an essence of the substituted hydrophobic residues in the primary resistance mutation. In addition, it is in accordance with the fact that the binding pocket of the HIV-1 protease is considerably hydrophobic. However, the magnitude of ΔE_{elec} (Table 2) should also be taken into consideration. Differences in the electrostatic components between the wt and each mutant show an energy loss of −1.10 kcal/mol for V82F, −4.41 kcal/mol for I84V, and −8.19 kcal/mol for V82F/I84V, suggesting that unfavorable interactions arose from the mutations. In terms of the magnitude, the loss of the nonbonded energy changes correlates well with the volume change of the interior cavity (ΔV in Table 1) induced by the mutation.

Effect of Mutation to the Binding in the Catalytic Domain. Residues in the binding domain of HIV-1 PR such as the catalytic triad and the flap region allow for several important hydrogen bonds to the main-chain RTV to be formed. The hydrogen bonding was determined using the following criteria: (i) a distance between donor and acceptor heavy atoms ≤ 3.5 Å, (ii) an angle of donor−H−acceptor ≥ 120°, and (iii) a percentage of occurrence in the simulations. From the histogram in Figure 9, six hydrogen bonds of the wt complex exist over a 90% occurrence frequency, whereas the single and the double mutants have five and four hydrogen bonds, respectively. Hydrogen bonding between the catalytic residues Asp25/Asp25′ and the OH of RTV denoted by d2, d3, and d4 is apparently strong. Particularly, d2 and d4 fluctuate in a range of 2.6−2.8 Å for the distance and 164−172° for the angle in all four MD trajectories. Moreover, hydrogen bonds d1 and d5 have the same magnitude in terms of the observed quantities. The significant difference may be depicted by d6, which is a hydrogen bond between D29 and the P3 subsite. The hydrogen bond is considerably weak and appears only in the wt complex.

CONCLUSION

We have studied the structure, dynamics, and free energies of binding of wild-type and primary resistance mutants, V82F, I84V, and V82F/I84V, HIV-1 protease complexed with ritonavir. Overall, structures of the enzyme and the hydrogen bonding of the catalytic residues to ritonavir are similar in all four complexes. On the basis of the MD data, the tip of the HIV-1 protease flap of the double mutant has the greater degree of opening with respect to that of the wild type and the two single mutants. The greatest conformational changes in the catalytic binding domain also took place on the double mutant complex. The substituted residues of the resistance mutants require a hydrophobic property to maintain the interactions in the binding pocket. The computed free energy of binding using the solvent continuum model is in good agreement with the experimental inhibition constant. Those changes induced by the mutations are free of energy penalties for the binding of the drug and are responsible for the loss of the drug's susceptibility.

ACKNOWLEDGMENT

Financial support by the Thailand Research Fund and the generous supply of computer time by Computational Chemistry Unit Cell (CCUC) and the Faculty Facility are gratefully acknowledged.

REFERENCES AND NOTES

(1) Hellen, C. U.; Krausslich, H. G.; Wimmer, E. Proteolytic Processing of Polyproteins in the Replication of RNA Viruses. *Biochemistry* **1989**, *28*, 9881−9890.

(2) Kohl, N. E.; Emini, E. A.; Schleif, W. A.; Davis, L. J.; Heimbach, J. C.; Dixon, R. A.; Scolnick, E. M.; Sigal, I. S. Active Human Immunodeficiency Virus Protease Is Required for Viral Infectivity. *Proc. Natl. Acad. Sci. U.S.A.* **1988**, *85*, 4686−4690.

(3) Swanstrom, R.; Erona, J. Human Immunodeficiency Virus Type-1 Protease Inhibitors: Therapeutic Successes and Failures, Suppression and Resistance. *Pharmacol. Ther.* **2000**, *86*, 145−170.

(4) Wlodawer, A.; Miller, M.; Jaskolski, M.; Sathyanarayana, B. K.; Baldwin, E.; Weber, I. T.; Selk, L. M.; Clawson, L.; Schneider, J.; Kent, S. B. Conserved Folding in Retroviral Proteases: Crystal Structure of a Synthetic HIV-1 Protease. *Science* **1989**, *245*, 616−621.

(5) Kempf, D. J.; Marsh, K. C.; Denissen, J. F.; McDonald, E.; Vasavanonda, S.; Flentge, C. A.; Green, B. E.; Fino, L.; Park, C. H.; Kong, X. P. ABT-538 is a Potent Inhibitor of Human Immunodeficiency Virus Protease and Has High Oral Bioavailability in Humans. *Proc. Natl. Acad. Sci. U.S.A.* **1995**, *92*, 2484−2488.

(6) Prabu-Jeyabalan, M.; Nalivaika, E.; Schiffer, C. A. Substrate Shape Determines Specificity of Recognition for HIV-1 Protease: Analysis of Crystal Structures of Six Substrate Complexes. *Structure* **2002**, *10*, 369−381.

(7) Lepsik, M.; Kriz, Z.; Havlas, Z. Efficiency of a Second-Generation HIV-1 Protease Inhibitor Studied by Molecular Dynamics and Absolute Binding Free Energy Calculations. *Proteins* **2004**, *57*, 279−293.

(8) Ohtaka, H.; Freire, E. Adaptive Inhibitors of the HIV-1 Protease. *Prog. Biophys. Mol. Biol.* **2005**, *88*, 193−208.

(9) Nair, A. C.; Bonin, I.; Tossi, A.; Wels, W. J.; Miertus, S. Computational Studies of the Resistance Patterns of Mutant HIV-1 Aspartic Proteases towards ABT-538 (Ritonavir) and Design of New Derivatives. *J. Mol. Graphics Modell.* **2002**, *21*, 171−179.

(10) Velazquez-Campoy, A.; Kiso, Y.; Freire, E. The Binding Energetics of First- and Second-Generation HIV-1 Protease Inhibitors: Implications for Drug Design. *Arch. Biochem. Biophys.* **2001**, *390*, 169−175.

(11) Ala, P. J.; Huston, E. E.; Klabe, R. M.; Jadhav, P. K.; Lam, P. Y.; Chang, C. H. Counteracting HIV-1 Protease Drug Resistance: Structural Analysis of Mutant Proteases Complexed with XV638 and SD146, Cyclic Urea Amides with Broad Specificities. *Biochemistry* **1998**, *37*, 15042−15049.

(12) Todd, M. J.; Luque, I.; Velazquez-Campoy, A.; Freire, E. Thermodynamic Basis of Resistance to HIV-1 Protease Inhibition: Calorimetric Analysis of the V82F/I84V Active Site Resistant Mutant. *Biochemistry* **2000**, *39*, 11876−11883.

(13) Xie, D.; Gulnik, S.; Gustchina, E.; Yu, B.; Shao, W.; Qoronfleh, W.; Nathan, A.; Erickson, J. W. Drug Resistance Mutations Can Effect Dimer Stability of HIV-1 Protease at Neutral pH. *Protein Sci.* **1999**, *8*, 1702−1707.

(14) Case, D. A.; Pearlman, J. W.; Caldwell, T. E.; Cheatham, J., III; Wang, W. S.; Ross, C. L.; Simmerling, T. A.; Darden, K. M.; Merz, R. V.; Stanton, A. L.; Cheng, J. J.; Vincent, M.; Crowley, V.; Tsui, H.; Gohlke, R. J.; Radmer, Y.; Duan, J.; Pitera, I.; Massova, G. L.; Seibel, U. C.; Singh, P. K.; Kollman, P. A. *AMBER 7*; University of California: San Francisco, CA, 2002.

(15) Davis, M. E.; Madura, J. D.; Luty, B. A.; Mccammon, J. A. Electrostatics and Diffusion of Molecules in Solution − Simulations

with the University-of-Houston-Brownian Dynamics Program. *Comput. Phys. Commun.* **1991,** *62*, 187−197.
(16) Wittayanarakul, K.; Aruksakunwong, O.; Sompornpisut, P.; Sanghiran-Lee, V.; Parasuk, V.; Pinitglang, S.; Hannongbua, S. Structure, Dynamics and Solvation of HIV-1 Protease/Saquinavir Complex in Aqueous Solution and Their Contributions to Drug Resistance: Molecular Dynamic Simulations. *J. Chem. Inf. Model.* **2005**, *45*, 300−308.
(17) Wittayanarakul, K.; Aruksakunwong, O.; Saen-oon, S.; Chantratita, W.; Parasuk, V.; Sompornpisut, P.; Hannongbua, S. Insights into Saquinavir Resistance in the G48V HIV-1 Protease: Quantum Calculations and Molecular Dynamic Simulations. *Biophys. J.* **2005**, *88*, 867−879.
(18) Nam, K. Y.; Chang, B. H.; Han, C. K.; Ahn, S. G.; No, K. T. Investigation of the Protonated State of HIV-1 Protease Active Site. *Bull. Korean Chem. Soc.* **2003**, *24*, 817−823.
(19) Won, Y. Binding Free Energy Simulations of the HIV-1 Protease and Hydroxyethylene Isostere Inhibitors. *Bull. Korean Chem. Soc.* **2000**, *21*, 1207−1212.
(20) Frisch, M. J.; Trucks, G. W.; Schlegel, H. B.; Scuseria, G. E.; Robb, M. A.; Cheeseman, J. R.; Zakrzewski, V. G.; Montgomery, J. A., Jr.; Stratmann, R. E.; Burant, J. C.; Dapprich, S.; Millam, J. M.; Daniels, A. D.; Kudin, K. N.; Strain, M. C.; Farkas, O.; Tomasi, J.; Barone, V.; Cossi, M.; Cammi, R.; Mennucci, B.; Pomelli, C.; Adamo, C.; Clifford, S.; Ochterski, J.; Petersson, G. A.; Ayala, P. Y.; Cui, Q.; Morokuma, K.; Malick, D. K.; Rabuck, A. D.; Raghavachari, K.; Foresman, J. B.; Cioslowski, J.; Ortiz, J. V.; Stefanov, B. B.; Liu, G.; Liashenko, A.; Piskorz, P.; Komaromi, I.; Gomperts, R.; Martin, R. L.; Fox, D. J.; Keith, T.; Al-Laham, M. A.; Peng, C. Y.; Nanayakkara, A.; Gonzalez, C.; Challacombe, M.; Gill, P. M. W.; Johnson, B. G.; Chen, W.; Wong, M. W.; Andres, J. L.; Head-Gordon, M.; Replogle, E. S.; Pople, J. A. *Gaussian 98*, revision A.11; Gaussian, Inc.: Pittsburgh, PA, 2001.
(21) Cornell, W. D.; Cieplak, P.; Bayly, C. I.; Kollman, P. A. Application of Resp Charges to Calculate Conformational Energies, Hydrogen-Bond Energies, and Free-Energies of Solvation. *J. Am. Chem. Soc.* **1993**, *115*, 9620−9631.
(22) Wang, J. M.; Wang, W.; Kollman, P. A. Antechamber: An Accessory Software Package for Molecular Mechanical Calculations. *Abstr. Pap. Am. Chem. Soc.* **2001**, *222*, U403.
(23) Jorgensen, W. L.; Chandrasekhar, J.; Madura, J. D.; Impey, R. W.; Klein, M. L. Comparison of Simple Potential Functions for Simulating Liquid Water. *J. Chem. Phys.* **1983**, *79*, 926−935.
(24) Cornell, W. D.; Cieplak, P.; Bayly, C. I.; Gould, I. R.; Merz, K. M.; Ferguson, D. M.; Spellmeyer, D. C.; Fox, T.; Caldwell, J. W.; Kollman, P. A. A Second Generation Force-Field for the Simulation of Proteins, Nucleic-Acids, and Organic-Molecules. *J. Am. Chem. Soc.* **1995**, *117*, 5179−5197.
(25) Berendsen, H. J. C.; Postma, J. P. M.; Vangunsteren, W. F.; Dinola, A.; Haak, J. R. Molecular-Dynamics with Coupling to an External Bath. *J. Chem. Phys.* **1984**, *81*, 3684−3690.
(26) Ryckaert, J. P.; Ciccotti, G.; Berendsen, H. J. C. Numerical-Integration of Cartesian Equations of Motion of a System with Constraints − Molecular-Dynamics of N−Alkanes. *J. Comput. Phys.* **1977**, *23*, 327−341.
(27) York, D. M.; Darden, T. A.; Pedersen, L. G. The Effect of Long-Range Electrostatic Interactions in Simulations of Macromolecular Crystals − A Comparison of the Ewald and Truncated List Methods. *J. Chem. Phys.* **1993**, *99*, 8345−8348.
(28) Gilson, M. K.; Sharp, K. A.; Honig, B. H. Calculating the Electrostatic Potential of Molecules in Solution: Method and Error Assessment. *J. Comput. Chem.* **1987**, *9*, 327−335.
(29) Sitkoff, D.; Sharp, K. A.; Honig, B. Accurate Calculation of Hydration Free-Energies Using Macroscopic Solvent Models. *J. Phys. Chem.* **1994**, *98*, 1978−1988.
(30) Rocchia, W.; Alexov, E.; Honig, B. Extending the Applicability of the Nonlinear Poisson−Boltzmann Equation: Multiple Dielectric Constants and Multivalent Ions. *J. Phys. Chem. B* **2001**, *105*, 6507−6514.
(31) Villa, J.; Strajbl, M.; Glennon, T. M.; Sham, Y. Y.; Chu, Z. T.; Warshel, A. How Important Are Entropic Contributions to Enzyme Catalysis? *Proc. Natl. Acad. Sci. U.S.A.* **2000**, *97*, 11899−11904.
(32) Kuhn, B.; Kollman, P. A. Binding of a Diverse Set of Ligands to Avidin and Streptavidin: An Accurate Quantitative Prediction of Their Relative Affinities by a Combination of Molecular Mechanics and Continuum Solvent Models. *J. Med. Chem.* **2000**, *43*, 3786−3791.
(33) Perryman, A. L.; Lin, J. H.; McCammon, J. A. HIV-1 Protease Molecular Dynamics of a Wild-Type and of the V82F/I84V Mutant: Possible Contributions to Drug Resistance and a Potential New Target Site for Drugs. *Protein Sci.* **2004**, *13*, 1108−1123.
(34) Liang, J.; Edelsbrunner, H.; Woodward, C. Anatomy of Protein Pockets and Cavities: Measurement of Binding Site Geometry and Implications for Ligand Design. *Protein Sci.* **1998**, *7*, 1884−1897.

CI060090C